Journal of Zhejiang University-SCIENCE A (Applied Physics & Engineering) 2023 24(10):912-924
www.jzus.zju.edu.cn; www.springer.com/journal/11582
E-mail: jzus_a@zju.edu.cn

Research Article

https://doi.org/10.1631/jzus.A2200550

Experimental investigation of the thermal insulation performance of Ce/Si/Ti oxide heat-reflective coating

Rui SU, Yue LV, Qian SU✉, Yanfei PEI

School of Civil Engineering, Southwest Jiaotong University, Chengdu 610031, China

Abstract: To solve the problem of deformation and cracking of ballastless track slab under temperature load, a composite oxide and a series of heat-reflective coating samples were prepared. At the microscopic level, the elemental composition and optical properties of the materials prepared were analyzed by Fourier transform infrared spectroscopy and ultraviolet-visible spectroscopy, and the feasibility of Ce/Si/Ti oxide as functional fillers for heat-reflective coatings of track slabs was demonstrated. At the macro level, by designing and assembling an indoor sunlight simulation test device, the surface and internal temperatures of the coated and uncoated concrete specimens were analyzed and studied, and the macroscopic cooling effect of the coatings was evaluated. Also, to study the engineering application effect of the track slab thermal insulation reflective coating, COMSOL was used to build a 3D calculation model of the heat transfer deformation of the ballastless track slab structure. The research results showed that: Ce/Si/Ti oxide has strong reflectivity and can reflect 95% of infrared light; it has good ultraviolet (UV) shielding ability and can absorb more than 65% of the UV light. The TiO_2 coating can reduce the temperature of the concrete surface by 6–11 ℃ and that of the inside of the concrete by 10–14 ℃; the cooling effect decreases evenly with the increase of air temperature. The Ce/Si/Ti oxide coating can reduce the surface temperature of the concrete by 16 ℃ and that of the inside of the concrete by 15 ℃. In addition, the cooling effect is basically not affected by the air temperature, and it changes non-linearly with the increase of the Ce/Si/Ti oxide content. Numerical calculation shows that the heat reflective coating can reduce the surface temperature and internal temperature difference of the track slab by 11.54–21.31 ℃, and the vertical displacement of the track slab can be reduced by about 35%–70%. Considering the cooling effect, the adhesion strength, and the engineering application effect of the coating, the optimal doping amount of Ce/Si/Ti oxide is 40%, and that coating is the most suitable for use as a ballastless track heat reflective coating.

Key words: Track slab; Solar radiation; Thermochromic coating; Cooling performance

1 Introduction

Temperature loading is the main factor causing warping and arching of ballastless track structures in high-speed railways and it seriously affects the durability and stability of such structures. Zeng et al. (2018) established an analytical model for the temperature field of double-block ballastless track slabs based on solar radiation theory and boundary heat exchange theory, to analyze the effect of geographical latitude on the temperature field of ballastless track slabs. Liu et al. (2020) developed a computational model for a ballastless track pre-stressed concrete simply supported box girder and proposed a connection between temperature and deformation in the beam-rail system and the spatial and temporal laws of temperature stress distribution within the track slab. Yu et al. (2019) used long-term meteorological statistics to establish a calculation model for the force deformation of ballastless track slabs under long-term temperature loading. Chen et al. (2020) built a model based on the transverse shear test and cohesive zone model for simulating the occurrence of damage, crack development, and interfacial bond failure at the interface between track slab and asphalt concrete waterproofing layer under the effect of temperature load. The calculation results showed that the interfacial bond state between track slab and asphalt concrete waterproofing

✉ Qian SU, suqian@126.com
Rui SU, https://orcid.org/0009-0005-3411-537X
Qian SU, https://orcid.org/0009-0007-8260-0016

Received Nov. 16, 2022; Revision accepted Jan. 16, 2023; Crosschecked Aug. 15, 2023

layer varies greatly by temperature and that the interfacial bond state has a greater impact on the dynamic performance of ballastless track structure. Fu et al. (2020) conducted on-site vibration tests and temperature deformation monitoring of ballastless track structures to comparatively study the mechanical behavior of asphalt concrete under train load and temperature load. The tests showed that the asphalt concrete bottom dealt with the tensile state under both train load and temperature load, but the temperature change had more significant effect on the force state of the asphalt concrete structure, especially near the expansion joints.

The remedial measures for temperature damage in ballastless track structures are divided into active and passive protection. Passive protection includes pins in the track slab to limit the deformation of the slab, injection of cementitious material at the bottom of the slab to enhance the bond between the slab and the mortar layer, and release of the stress on the slab during the high temperature season. Active protection includes the application of heat-reflective coatings to the surface of the rail panels. Research into heat-reflective coatings in rail transport is in its early stages. Jiang et al. (2020) developed a phase-change thermal insulation reflective coating which, through full scale tests, indoor thermal insulation tests, and theoretical calculations, was shown to be effective in reducing the rate of concrete heating and the surface temperature in high temperature environment, as well as in reducing the temperature gradient and thermal deformation of track slabs in high temperature environment. Li et al. (2021) used hollow polymer microspheres dispersed in a fluorocarbon coating to prepare a coating capable of reflecting most of the thermal radiation and blocking heat transfer. They demonstrated, through tests, that the coating was able to reduce the track slab surface temperature by 10% and the track slab thermal deformation by up to 19%. Zhang et al. (2020) developed a metal-ceramic anti-corrosion coating made of inorganic phosphate and metallic aluminium. This coating not only reduced the temperature stress and thermal deformation inside the track slab but also protected the surface of the track slab from erosion. They analyzed the thermal insulation effect of the coating under different coating thicknesses through track slab thermal insulation tests and theoretical calculations.

Heat reflective coatings are widely used in construction and highway applications (Levinson et al., 2007; Ferrari et al., 2015; Jelle et al., 2015; Zheng et al., 2015; Park and Krarti, 2016; Chen et al., 2019; Al-Naghi et al., 2020). Zheng et al. (2015) used methacrylic resin as a binder, titanium oxide and azodiazepine black as pigments, and hollow glass beads as functional fillers to prepare an asphalt pavement coating capable of cooling, anti-slip, and anti-glare. Indoor and outdoor tests showed that the coating could effectively reduce the surface temperature of an asphalt pavement. To fully exploit the cooling efficiency of the material, experts are beginning to design and study multilayer coatings. Chen et al. (2019) produced a multi-structured thermal barrier coating capable of reducing rutting and preventing glare on asphalt pavements using modified epoxy resin, silica, titanium dioxide, and hollow glass beads. They showed, by indoor thermal insulation experiments, that the coating was able to reduce the temperature of asphalt pavements by 13.25 ℃. Jiang et al. (2019) designed and developed an asphalt pavement cooling coating consisting of an infrared transmitting layer, strong reflective layer, and heat insulation layer. The main components of the coating were organosilicon modified propionate emulsion, rutile titanium dioxide, hollow microbeads, water, and film-forming additives. Indoor test results showed that it could reduce the temperature inside the specimen by 13 ℃ and meet the standard requirements of anti-slip, water resistance, acid and alkali resistance, and wear resistance. Saber (2021) tested the effect of varying degrees of washing as well as rain erosion and natural weathering on the solar reflectivity of heat reflective coatings, showing that dust on the surface of the coating affects the reflection of short-wave sunlight, increasing the reflectivity of the coating for short-wave sunlight by 5% under wind action and by 45% after washing. Guo et al. (2012) built a thermal insulation coating test house in a hot-summer and cold-winter region to test the thermal insulation performance of reflective thermal insulation coating. The experimental results showed that the thermal insulation coating was able to reduce the temperature of the building's exterior walls by 8–10 ℃ and was able to save about 5.8 kWh/m^2 of electricity for air conditioning each month. Thejus et al. (2021) synthesised the $LiMg_{1-x}Co_xPO_4$ series of inorganic pigments, which are capable of reflecting 55%

of sunlight and 67% of near-infrared light in heat reflective coatings, and have good corrosion resistance, making them a better insulating and anti-corrosion coating for buildings. Malz et al. (2020) investigated the use of infrared reflective coatings in the building field and used heat transfer theory to calculate that infrared reflective coatings can reduce the interior heat loss by 18%–20%.

To enhance the applicability of the coating to high-speed railway ballastless track slabs, this study develops a heat reflective coating for track slabs with good ultraviolet (UV) shielding, strong adhesion, and high reflectivity based on the existing coating technology, according to the characteristics of high-speed railway operation, ballastless track structure, and climate environment. The thermal insulation experiment of the coating was carried out indoors to study the effect of the coating on the temperature distribution inside the concrete and to verify the feasibility of its application to the ballastless track slabs of high-speed railways.

2 Material system

2.1 Coating system design

The heat reflective coating of the high-speed railway track slab consists of a top layer, a middle layer, and a bottom layer. Epoxy resin has high bond strength and chemical resistance, but its weather resistance is poor; the specific parameters are presented in Table 1. Therefore, epoxy resin is chosen as the base layer of the coating structure to increase the bonding between the concrete track slab and the coating structure. The top layer is able to isolate dust, water, acid, alkali, and UV rays from the natural environment and protects the coating from environmental erosion. The middle layer has the function of reflecting sunlight and blocking heat transfer. In order to make the overall bonding and elasticity of the top and middle layers consistent, the coating base material for the top and middle layers is polytrifluoroethylene resin (PEVE), which has a strong C–F bond as a backbone and has good heat resistance, chemical resistance, and cold resistance.

Ce/Si/Ti oxide is a reflective material and pigment for heat reflective coating formed by wrapping SiO_2 and CeO_2 on the surface of TiO_2. Silicon dioxide aerogel and hollow glass beads are thermal insulation materials. Phase-change particles were used as energy storage and temperature regulation materials. In this experiment, 10 types of heat reflective coatings for track slabs were designed and the effect of the coatings on the behaviour of the temperature field inside the track slabs was investigated. The specific formulations and parameters of the coatings are shown in Table 2.

2.2 Preparation of Ce/Si/Ti oxide

Preparation of Ce/Si/Ti oxide was by an acid-base neutralization method. Firstly, 1 mol of rutile titanium dioxide was dispersed in 10 L of deionized water and 0.01 mol of $(NaPO_3)_6$ was added, and the pH of the suspension was adjusted to 9. That's because after many comparative tests, 0.01-mol $(NaPO_3)_6$ was found to be the most beneficial to the dispersion of the titanium oxide particles. If $(NaPO_3)_6$ was less than 0.01 mol, it resulted in poor dispersion of the titanium oxide and reduced production of Ce/Si/Ti oxide; if it was more than 0.01 mol, there were more impurities in the final product and they were difficult to remove. Moreover, several tests in the laboratory indicated that when the PH of the suspension reached 9, the titanium oxide particles were the best dispersed and most fully reacted with the assistance of 0.01-mol $(NaPO_3)_6$, and the highest yield of Ce/Si/Ti oxide could be achieved.

The suspension was heated to 90 ℃ and stirred in the reaction vessel for 2 h. Then, a constant pressure funnel was used to drop in 0.1-mol/L Na_2SiO_3 (150 mL) and 0.1-mol/L H_2SO_4 solution, keeping the temperature and pH in the reaction vessel constant. Next, a constant pressure funnel was used to drop in 0.1-mol/L $Ce(SO_4)_2$ and 0.1-mol/L NaOH solution, keeping the temperature and pH in the reaction vessel constant. Then, the reaction was aged for 6 h at a temperature of 90 ℃ and a speed of 300 r/min. Finally, the suspension was filtered, dried, and crushed to obtain Ce/Si/Ti oxide powder.

Table 1 Parameters of the resin (25 ℃)

Epoxy resin			Fluorocarbon resin		
Appearance	Density (g/cm^3)	Viscosity (mPa·s)	Appearance	Density (g/cm^3)	Viscosity (mPa·s)
Colorless transparent	1.10–1.12	9000–12000	Colorless transparent	1.74–1.77	7500–8000

Table 2 Formulations of the coatings

Type of coating	No.	Top layer		Middle layer		Bottom layer	
		Component	Thickness (μm)	Component	Thickness (μm)	Component	Thickness (μm)
Heat insulation	S1	Fluorocarbon resin+50% TiO_2+additive	30	Fluorocarbon resin+10% SiO_2+10% PCM+additive	200	Fluorocarbon resin+additive	30
	S2	Fluorocarbon resin+50% TiO_2+additive	30	Fluorocarbon resin+6% hollow glass beads+10% PCM+additive	200	Fluorocarbon resin+additive	30
	S3	Fluorocarbon resin+50% Ce/Si/Ti oxide+additive	30	Fluorocarbon resin+10% SiO_2+10% PCM+additive	200	Fluorocarbon resin+additive	30
	S4	Fluorocarbon resin+50% Ce/Si/Ti oxide+additive	30	Fluorocarbon resin+6% hollow glass beads+10% PCM+additive	200	Fluorocarbon resin+additive	30
Heat reflective	S5	Fluorocarbon resin+additive	30	Fluorocarbon resin+20% Ce/Si/Ti oxide+additive	200	Fluorocarbon resin+additive	30
	S6	Fluorocarbon resin+additive	30	Fluorocarbon resin+33% Ce/Si/Ti oxide+additive	200	Fluorocarbon resin+additive	30
	S7	Fluorocarbon resin+additive	30	Fluorocarbon resin+40% Ce/Si/Ti oxide+additive	200	Fluorocarbon resin+additive	30
	S8	Fluorocarbon resin+additive	30	Fluorocarbon resin+50% Ce/Si/Ti oxide+additive	200	Fluorocarbon resin+additive	30
	S9	Fluorocarbon resin+additive	30	Fluorocarbon resin+20% TiO_2+additive	200	Fluorocarbon resin+additive	30
	S10	Fluorocarbon resin+additive	30	Fluorocarbon resin+50% TiO_2+additive	200	Fluorocarbon resin+additive	30

PCM: phase change microcapsule

3 Experimental procedure

3.1 Experimental overview

The overall process of the test was to prepare the functional materials, prepare the coating, place the coating, and then test the thermal insulation capacity. The specific steps are shown in Fig. 1.

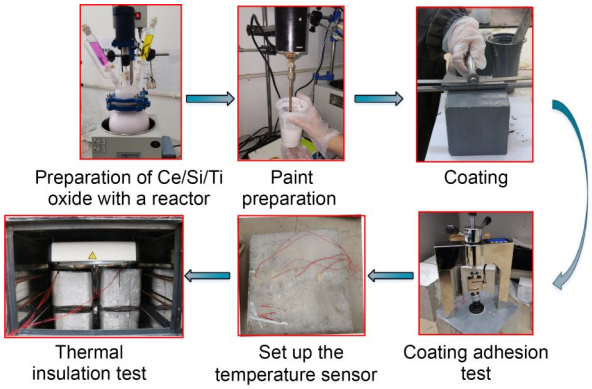

Fig. 1 General process of the tests

The general process of conducting this trial was as follows. Firstly, Ce/Si/Ti oxide powder was prepared in the reactor. Then, the defoamer, anti-settling agent, and film-forming additives were mixed with the resin in proportion. After that, the functional materials were dispersed in the resin and dispersed with a disperser at the same time to form the paint required for the test. Next, a coating of paint was applied to the top surface of the concrete specimen in accordance with GB/T 1727–2021 (SAMR, 2021). Then, the coating adhesion strength was tested according to ASTM D4514–12 (ASTM, 2012) and GB/T 5210–2006 (AQSIQ, 2006). Afterwards, temperature sensors were placed in the concrete specimens and a thermal insulation membrane was applied to the bottom and sidewalls of the specimens. Finally, the thermal insulation of the coating was tested with four levels of temperature loading: 50, 55, 60, and 66 °C, with each heat cycle being 4 h and the total test cycle being 16 h.

3.2 Infrared heating device and specimen

To investigate the internal temperature distribution law of concrete under the protection of coating, the sunlight simulation device (Fig. 2) developed by Su et al. (2023) was used to simulate the real light and heat environment. A concrete specimen with the size of 20 cm×20 cm×20 cm was used to test the insulation

effect of the coating, and the temperature sensors were deployed in the interior of the concrete specimen, and the specific arrangement scheme is shown in Fig. 3.

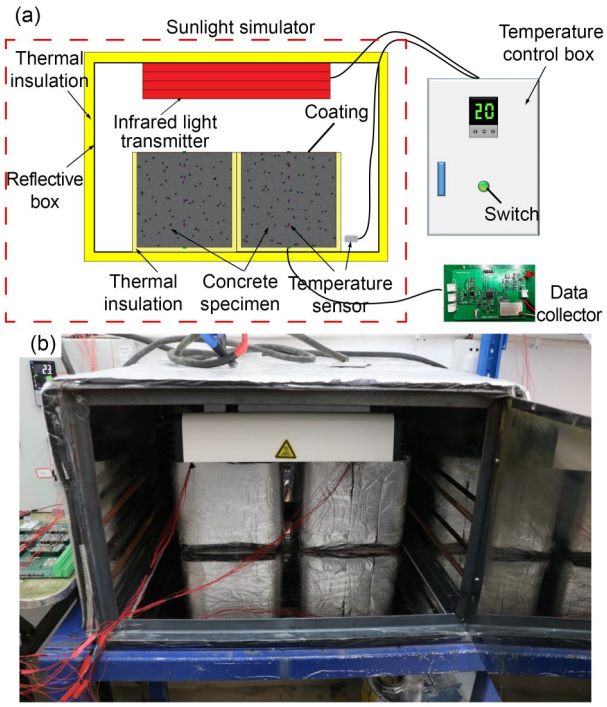

Fig. 2 Solar simulation system in the tests: (a) schema; (b) physical drawing

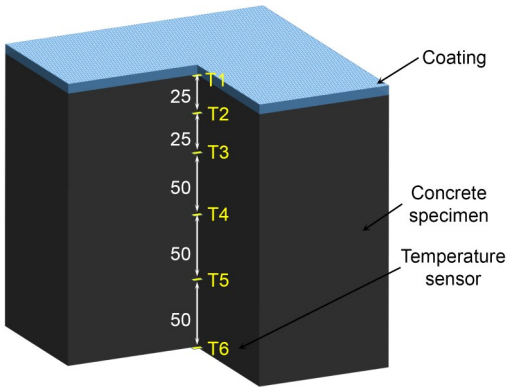

Fig. 3 Layout of the temperature sensors T1–T6 (unit: mm)

4 Results and discussion

4.1 Fourier transform infrared (FTIR) spectroscopy analysis

Fig. 4 illustrates the FTIR spectra of TiO_2 and Ce/Si/Ti oxide powders, where 468.25 cm^{-1} is the symmetric stretching vibrational absorption peak of Si–O–Si, 713.03–873.14 cm^{-1} is the symmetric stretching vibrational absorption peak of Ti–O–Ti and Ti–O, 1117.92 cm^{-1} is the vibrational absorption peak of Ce-O, 1419.13–1636.30 cm^{-1} is the symmetric vibrational absorption peak of O–H in water, and 3436.22 cm^{-1} is the antisymmetric telescopic vibrational absorption peak of O–H in water.

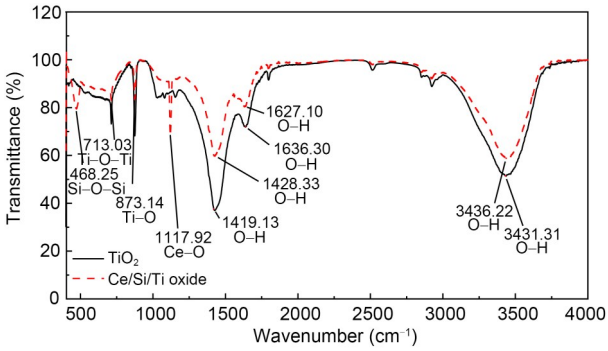

Fig. 4 FTIR spectra of TiO_2 and Ce/Si/Ti oxide powder

Comparison of the infrared (IR) spectra of titanium oxide and Ce/Si/Ti oxide reveals that the absorption peaks of hydroxyl groups become weaker after surface modification of titanium oxide, indicating a reduction in the water absorption of the surface modified titanium oxide (Ce/Si/Ti oxide). There are strong Ti–O and Ti–O–Ti absorption peaks on the surface of titanium oxide, by contrast the Ti–O and Ti–O–Ti absorption peaks on the surface of Ce/Si/Ti oxide are substantially less intense. Strong Si–O–Si and Ce–O absorption peaks appear on the surface of Ce/Si/Ti oxide, indicating that the TiO_2 surface is wrapped with SiO_2 and CeO_2 shells during the preparation of Ce/Si/Ti oxide. Fig. 4 shows that the reduction of hydrophilic groups on the surface of the Ce/Si/Ti oxides results in less adsorption of water and therefore the Ce/Si/Ti oxides are more easily dispersed and less prone to agglomeration when added to paints.

4.2 Optical characterization

The light reflectivity and light shielding properties of TiO_2 and Ce/Si/Ti oxide are shown in Figs. 5 and 6. As can be observed from Fig. 5, the reflectance of Ce/Si/Ti oxide for visible and far-infrared light is slightly reduced by up to 5% due to the sealing of SiO_2 and CeO_2 on the TiO_2 surface. The reflectance of Ce/Si/Ti oxide is about equal to that of TiO_2 in the

near-infrared (NIR) region, and the reflectance of Ce/Si/Ti oxide in the UV region is twice that of TiO_2. The reflectance patterns of Ce/Si/Ti oxide and TiO_2 for different wavelengths of light are generally consistent. Compared to TiO_2, Ce/Si/Ti oxide has significantly enhanced the reflectance for UV light and slightly reduced the reflectance for visible and IR light, but the reduction in reflectance for visible and IR light is less than 5%. In Fig. 6, it can be observed that the development pattern of absorption rate of Ce/Si/Ti oxide and TiO_2 for different wavelengths of ultraviolet B (UVB) is basically the same. However, the absorption ability for UVB of Ce/Si/Ti oxide is significantly improved and is twice as high as that of TiO_2; the maximum absorption rate for UVB of Ce/Si/Ti oxide is 82%, while that of TiO_2 is 40%. UVB is the main factor leading to the ageing and cracking of the coating and the reduction of the thermal insulation capacity of the coating. The absorption of UVB by TiO_2 is only 30%, while that by Ce/Si/Ti oxide is as high as 70%. In conclusion, the Ce/Si/Ti oxide without affecting its anti-thermal ability, not only has the excellent heat reflectivity of TiO_2, but also possesses the thermal stability of SiO_2 and the UV shielding property of CeO_2, and thus can effectively reduce the adverse effect of UVB on the durability of the coating and extend the service life of the coating.

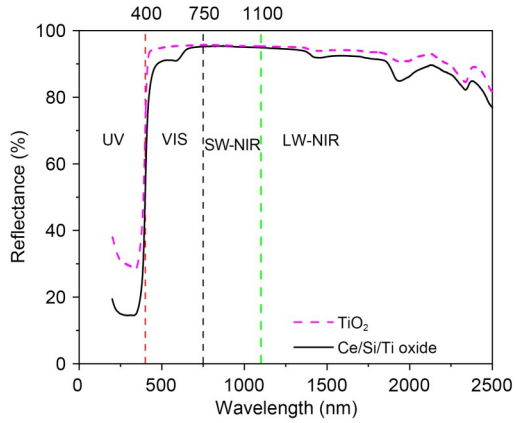

Fig. 5 Reflection spectra of TiO_2 and Ce/Si/Ti oxide powder. VIS: visible; SW-NIR: short wave near-infrared; LW-NIR: long wave near-infrared

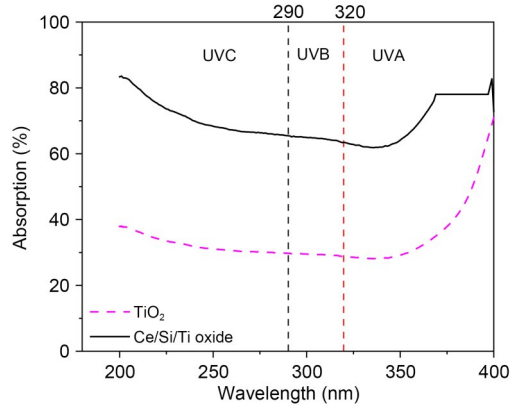

Fig. 6 Absorption spectra of TiO_2 and Ce/Si/Ti oxide powder. UVA: ultraviolet A; UVC: ultraviolet C

4.3 Temperature control efficiency

4.3.1 Heating process

Fig. 7 demonstrates the internal temperature variation rules of concrete specimens with different coatings. With the change of ambient temperature, the temperature variation rules and values of T5 and T6 are always similar. The surface temperature of the uncoated specimen rises faster, and the temperature difference between T1–T6 is larger, due to the fact that concrete is a poor conductor of heat. When the surface of the concrete is heated, the surface temperature of the concrete will rise rapidly and be equal to the ambient temperature, while the internal temperature of the concrete rises slower with the increase of the depth, and this is also the main reason for the cracking of high-speed railroad track slab. By spraying a coating material on the surface of the concrete to impede the absorption of heat from the surface of the concrete, the temperature difference and the rate of temperature rise within the concrete are reduced. Comparing the test results of the uncoated specimen with the S1–S4 specimens, it is easy to find that the availability of the coating reduces the amount of heat transfer from the concrete surface or reduces the rate of heat entering the concrete specimens.

By comparing S1 and S3, S2 and S4 separately, it can be obtained that the cooling effect of Ce/Si/Ti oxide coating as a top layer is about the same as that of TiO_2 coating as a top layer, indicating that although the Ce/Si/Ti oxide surface is covered by SiO_2 and CeO_2, resulting in a reduction of its IR reflectance by about 2%, the macroscopic heat reflectivity of Ce/Si/Ti oxide is not affected.

The temperature rise process at different depths within the heat reflective coated specimens is shown in Fig. 8. Comparison of S5–S9 shows that the same content of TiO_2 and Ce/Si/Ti oxide heat reflective

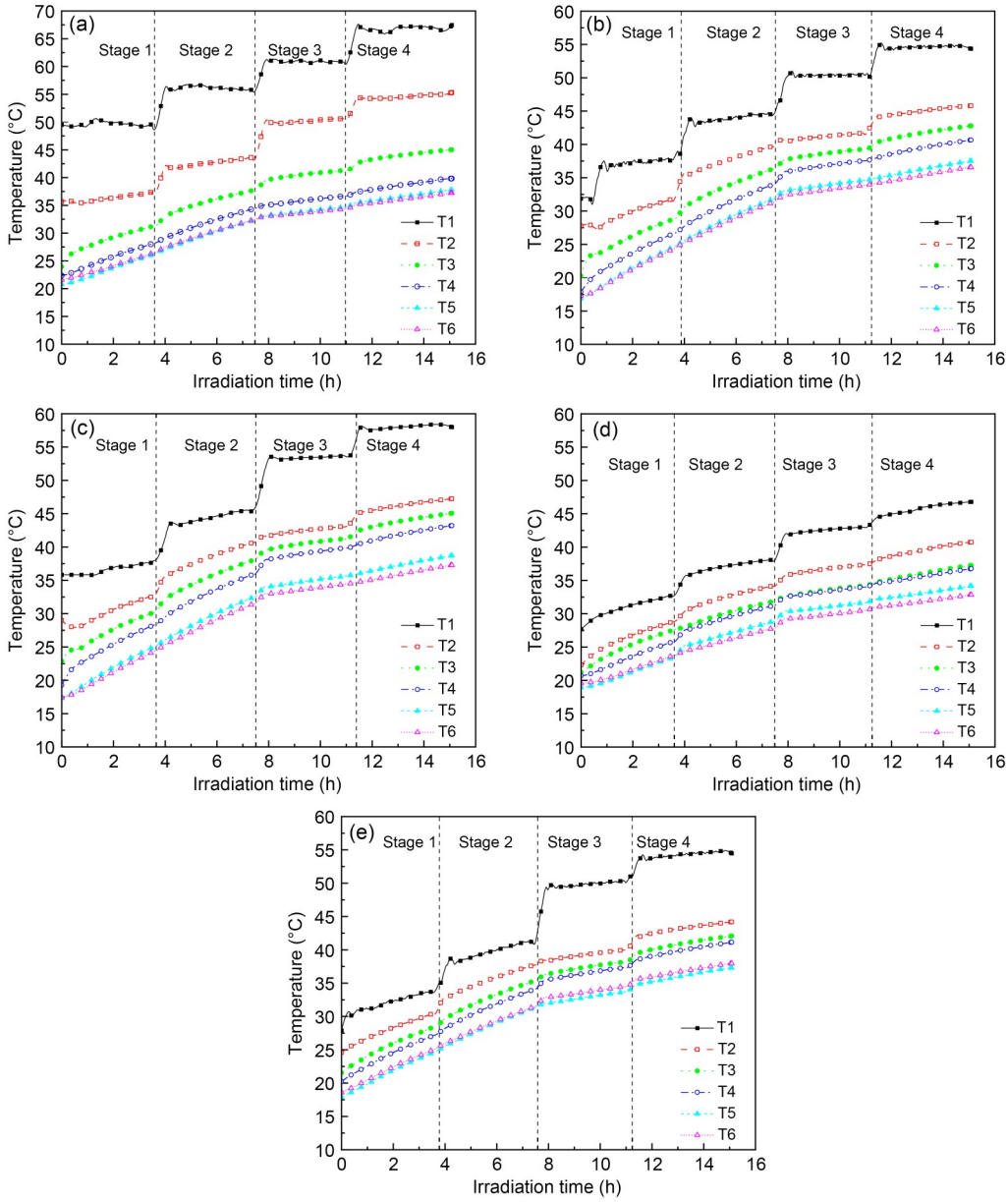

Fig. 7 Temperature variation of thermal insulation coating specimens: (a) uncoated concrete; (b) S1; (c) S2; (d) S3; (e) S4

coatings have basically the same effect on the surface cooling of concrete specimens and are capable of reducing the surface temperature of concrete by 6–16 ℃. By comparing Figs. 7 and 8, it is found that the surface cooling effect and reduction of temperature gradient is better with the heat reflective coating. This is because the heat in the concrete comes mainly from solar radiation and ambient heat exchange, and the concrete gets more heat from solar radiation; thus, the cooling effect of the heat reflective coating will be better.

4.3.2 Temperature difference

The internal temperature difference of the concrete specimens can be calculated according to Eq. (1) and the results are shown in Fig. 9.

$$\Delta T_i = T_i - T_{i+1}, \tag{1}$$

where i is the temperature sensor measurement point number, ΔT_i is the internal temperature difference of the concrete, and T_i is the concrete temperature at different depths.

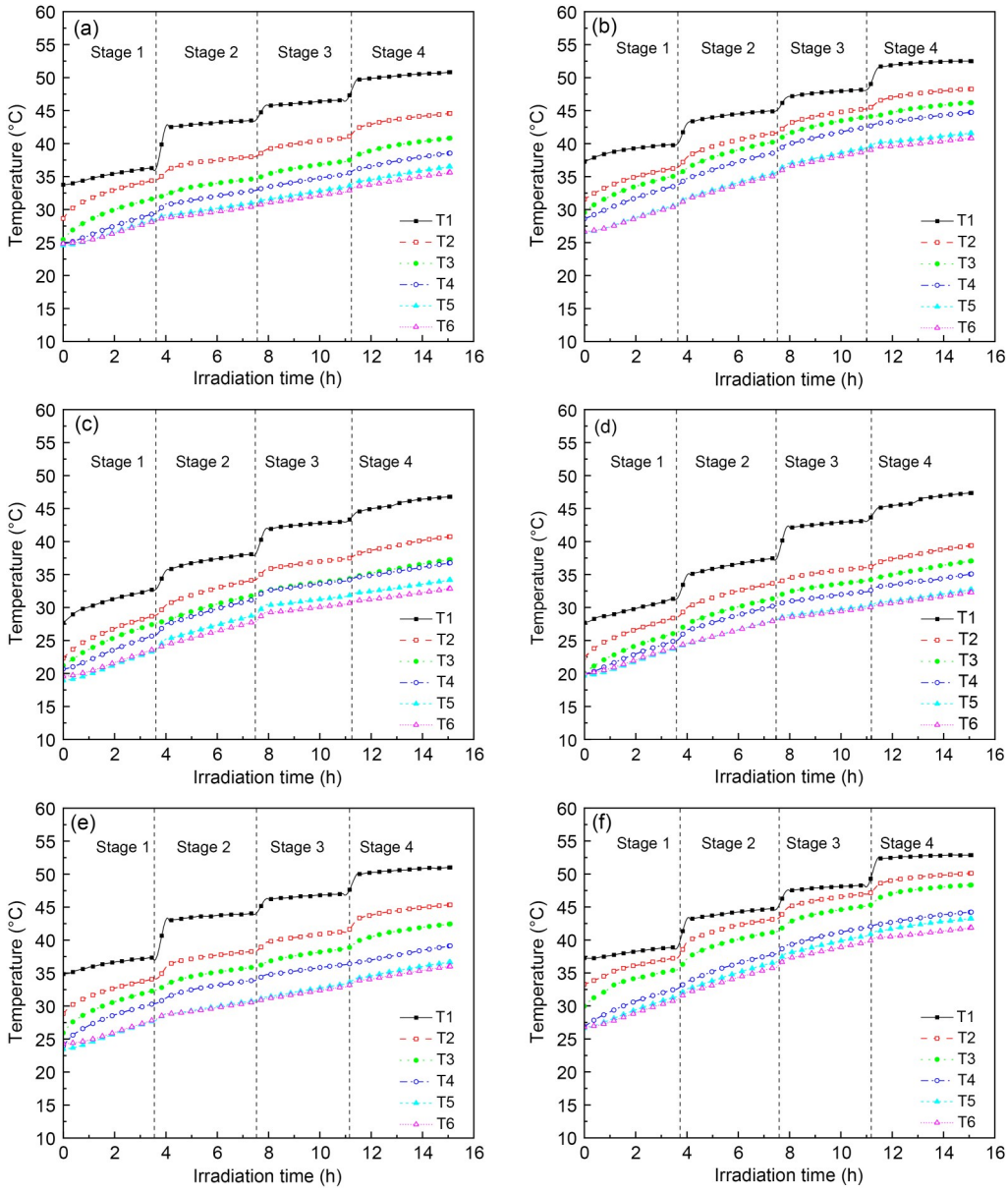

Fig. 8 Temperature variation of thermal reflective coating specimens: (a) S5; (b) S6; (c) S7; (d) S8; (e) S9; (f) S10

The cumulative temperature difference within the uncoated concrete specimens is as high as 23.1 ℃ and the surface temperature difference is less influenced by the ambient temperature, which indicates that the thermal conductivity of concrete is less influenced by the ambient temperature. S1–S4 are reflective thermal insulation coatings; S1 and S2 have large changes in the internal temperature gradient of concrete with the increase of ambient temperature, with ΔT_1 having the greatest changes with the increase of ambient temperature, increasing by 60% and 30%, respectively; while S3 and S4 have smaller changes in the accumulated temperature difference with the ambient temperature, with the accumulated temperature difference increasing by 0.36 ℃ for every 1 ℃ rise of the average ambient temperature. This is because, compared with TiO_2, the Ce/Si/Ti oxide surface compounded with SiO_2 improves the overall thermal stability of the coating. S5–S10 are reflective coatings and a comparison of S5–S8 reveals that the Ce/Si/Ti oxide content is non-linear with the change in temperature gradient inside the concrete. The cumulative temperature difference inside the concrete is the lowest when the Ce/Si/Ti oxide contents are 33%

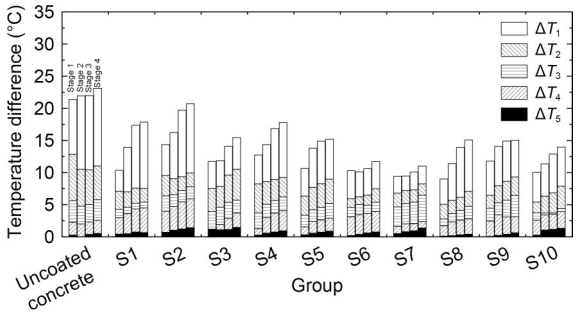

Fig. 9 Temperature gradient in concrete specimens

and 40% (S6 and S7). Comparing S1, S2, S10 and S3, S4, S8 respectively, it was found that the cumulative temperature difference of the thermal insulation coatings (S1–S4) was 1.3–2.0 times higher than that of the heat reflective coatings (S8 and S10). This is because the heat inside the concrete in a short period of time originates mainly from infrared radiation and the heat reflective coating is more conducive to reducing the temperature difference inside the concrete, reflecting that the TiO_2 and Ce/Si/Ti oxide contents have less influence on the temperature gradient.

4.4 Adhesion strength

The damage of the coatings in the adhesion test is shown in Fig. 10. S1, S2, S4, and S7 coatings are separated from the base concrete, which are adhesion damage; S3, S5, S6, S8, S9, and S10 coatings are pulled apart, which are cohesion damage. The pattern of coating damage shows that the results of the coating adhesion tests give a true and valid indication of the adhesion of coatings S1–S10.

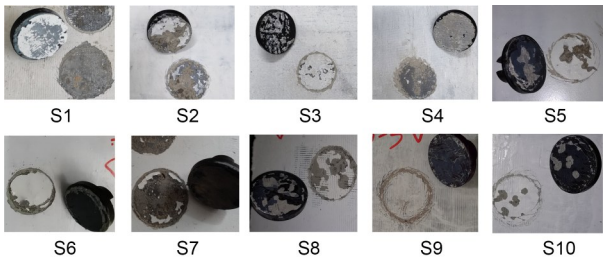

Fig. 10 Failure phenomenon of the coating

The coating adhesion strengths are shown in Fig. 11, where the lowest adhesion strengths are found for the thermal insulation coatings (S1–S4). In particular, when silica aerogel is added to the coatings, the coating adhesion strength decreases by 53%–57%. The adhesion strength of the reflective coatings (S5–S10) is greater, and the adhesion strength of the Ce/Si/Ti oxide coatings (S7) is higher than that of the TiO_2 coatings (S9 and S10). The adhesion strength of the Ce/Si/Ti oxide (S5–S8) varies non-linearly with the increasing Ce/Si/Ti oxide content, and the coating adhesion strength is the greatest when the Ce/Si/Ti oxide content is 40% (S7). In Fig. 10, the S7 coating is pulled apart completely when the coating is broken in the adhesion strength test, and it is confirmed that the interlayer bonding of the S7 coating is even better.

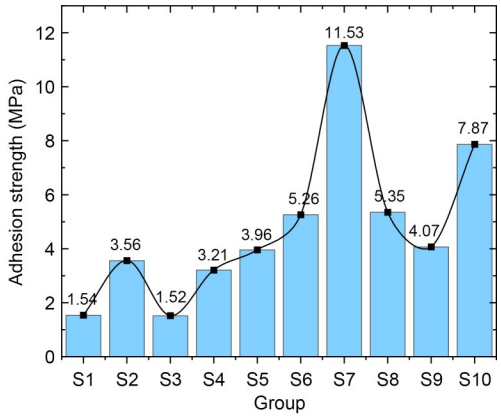

Fig. 11 Adhesion strengths of the coatings

5 Engineering application

To investigate the cooling effect of the coating on the track slab, a numerical calculation model proposed by Su et al. (2023) was used to analyze the distribution law of the internal temperature and deformation of the track slab under the protection of the coating. The initial ambient temperature in the calculation is 20 ℃ and the maximum temperature is 50 ℃. Temperature calculation time is 4 h. Material parameters used in the calculation are shown in Table 3.

5.1 Model verification

To verify the rationality of the computational model in this study, the temperature distribution of concrete specimens under 50-℃ ambient temperature was calculated and compared with the results of laboratory tests. The simulation results are shown in Fig. 12.

Fig. 12 compares the test results with the numerical calculations, and it is found that the difference between the internal temperature of the concrete specimens measured in the laboratory and the numerical

Table 3 Material properties

Component	Density (kg/m^3)	Elastic modulus (Pa)	Poisson's ratio	Thermal conductive coefficient (W/(m·K))	Heat transfer coefficient (W/(m^2·K))	Thermal expansion coefficient (K^{-1})
Track slab	2500	3.6×10^{10}	0.20	1.280	150.0	1×10^{-5}
Cement asphalt (CA) mortar	1500	9.0×10^{6}	0.34	0.930		
Supporting layer	2550	2.5×10^{10}	0.20	1.800		1×10^{-5}
Thermal insulation layer	300	5.0×10^{5}		0.085	10.0	
Coating	2300–2460				1.2–9.7	

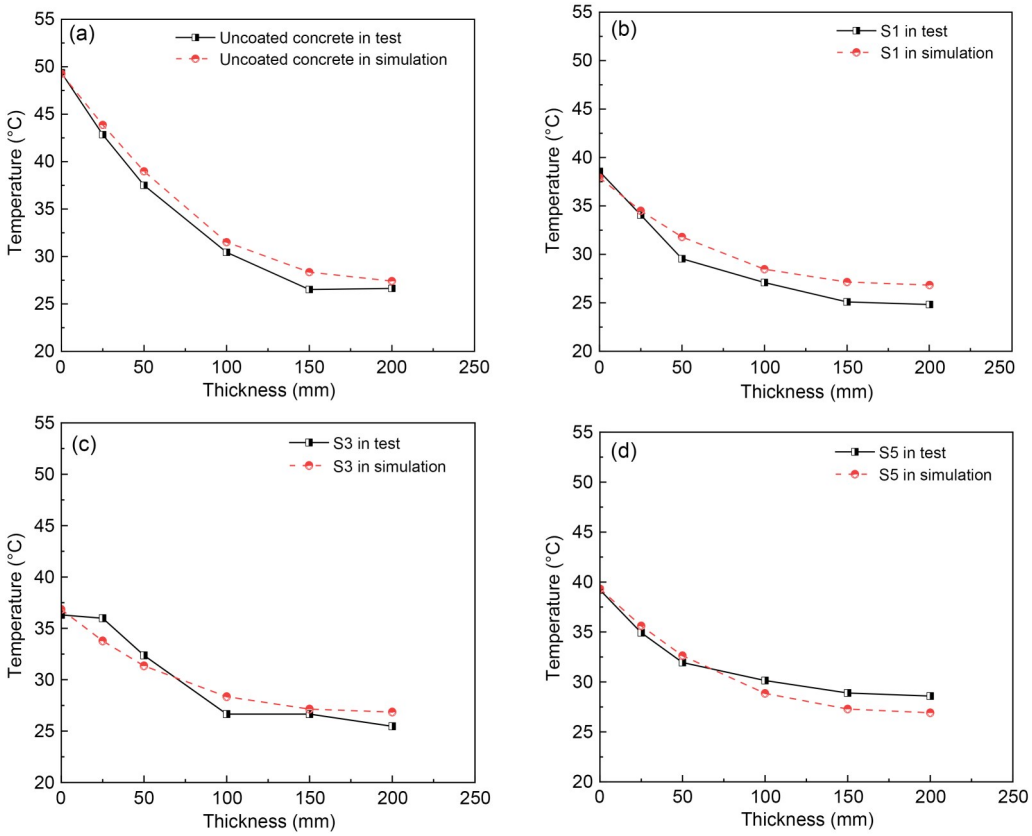

Fig. 12 Comparison of simulation and test results: (a) uncoated concrete; (b) S1; (c) S3; (d) S5

calculations is less than 7%, indicating that the numerical model is reliable and can accurately reflect the internal temperature of the concrete.

5.2 Temperature distribution of the track slab

The central cross-section of the track slab has a large temperature difference and, in engineering practice, thermal stresses and thermal deformations are generated inside the track plate during the hot summer. They result in arching of the track plate and thus damage to the ballastless track structure, where the centre of the track plate has the largest deformation and is the most easily damaged. The central cross-section of the track slab is thus chosen as a typical interface for analyzing the temperature distribution of the track slab under different conditions. The temperature distribution of the track slab without coating is shown in Fig. 13a; the temperature of the outer surface of the track slab is equal to the external ambient temperature and the temperature decreases sharply inwards, resulting in a large difference between the internal and surface temperatures of the track slab. According to Figs. 13b–13d, the surface temperature of the track slab decreases by different amounts after the coating is applied, and the highest temperature points appear at four corners of the track slab.

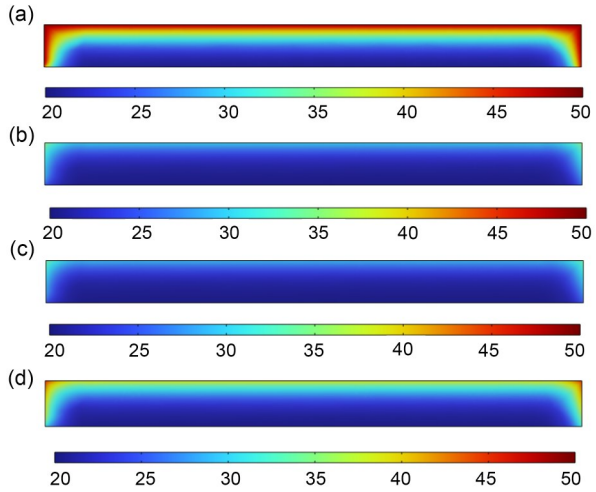

Fig. 13 Temperature distribution of track slab: (a) uncoated concrete; (b) S7; (c) S8; (d) S10 (unit: ℃)

Calculation results of the track slab temperature under different conditions are shown in Table 4. Without coating, the internal temperature difference of the track slab is as high as 29.62 ℃. The coating can reduce the difference between the surface and internal temperatures of the track by 11.54–21.31 ℃. Among them, S7 and S8 coatings have the best cooling effect, and can reduce the internal temperature differences of the track slab by 69.1% and 71.9% and the surface temperatures by 41.6% and 43.3%, respectively.

5.3 Deformation characteristics of the track slab

The layer has a different degree of relief to the deformation of the track slab and the specific values of the track slab deformation are shown in Table 5. In Table 5, the track slab coating can reduce the deformation of the track slab by about 35% to 70%, among which S7 and S8 coatings are the most effective in controlling the deformation of the track slab, reducing the deformation of the track slab by 66.0% and 69.8%, respectively, which is consistent with the results of the track slab temperature calculation.

In summary, the S7 coating has excellent temperature shielding properties, good adhesion properties, and track slab deformation control; therefore, the S7 coating is the most suitable as a thermal insulation coating for high-speed railway track slabs.

6 Conclusions

In this study, a composite titanium oxide heat reflective material was developed; different coatings were designed; laboratory samples were prepared. A series of indoor tests were carried out to test the thermal reflectivity, temperature control, and adhesion strength of the coating. The following conclusions were obtained from this study.

1. Ce/Si/Ti oxide has an IR reflectivity of 95% and can absorb more than 65% of UV light. The composite titanium oxide has good thermal reflectivity, thermal stability, and UV light shielding properties.

2. The test results show that the strong reflective coating can better reduce the temperature of the concrete surface and reduce the temperature difference inside the concrete. Ce/Si/Ti oxide can reduce the concrete surface temperature by 25% and can reduce the temperature difference inside the concrete by 15 ℃; its cooling ability is not affected by the ambient temperature and has good thermal stability.

Table 4 Summary of temperature calculation results of the track slab

Load condition	Surface temperature (℃)	Bottom temperature (℃)	Edge temperature (℃)	Internal temperature difference (℃)
Uncoated concrete	50.00	20.38	50.00	29.62
S1	34.36	20.21	40.48	14.15
S2	34.34	20.12	40.42	14.22
S3	32.74	20.10	39.48	12.64
S4	31.19	20.08	37.79	11.11
S5	35.85	20.16	42.94	15.69
S6	37.78	20.15	44.65	17.63
S7	29.22	20.07	35.36	9.15
S8	28.37	20.06	34.11	8.31
S9	34.91	20.14	41.72	14.05
S10	38.27	20.19	44.77	18.08

Table 5 Deformation calculation results of the track slab

Load condition	Deformation (mm)	Deformation reduction rate (%)
Uncoated concrete	1.06	
S1	0.53	50.0
S2	0.50	52.8
S3	0.49	53.8
S4	0.43	59.4
S5	0.60	43.4
S6	0.67	36.8
S7	0.36	66.0
S8	0.32	69.8
S9	0.56	47.2
S10	0.68	35.8

3. The coating adhesion test shows that the introduction of hollow glass beads and aerogel materials will reduce the adhesion strength of the coating and that the adhesion strength of Ce/Si/Ti oxide coating has a non-linear relationship with its content; when the content of Ce/Si/Ti oxide is 40%, the strength reaches the maximum of 11.53 MPa.

4. The finite element calculation results show that the coating can reduce the surface temperature and internal temperature difference of the track slab by 11.54–21.31 ℃. When the Ce/Si/Ti oxide content is 40%–50%, the cooling effect of the coating is excellent. It can reduce the surface temperature of the track slab by about 40%, the temperature difference by about 70%, and the vertical displacement of the track slab by about 70%.

5. Taking into account the thermal insulation rate of the coating, the internal temperature difference of the concrete, and the adhesion strength of the coating, as well as the deformation control effect of the track slab, the optimal amount of Ce/Si/Ti oxide is 40% and that coating is the most suitable for the thermal insulation coating of the track slab.

Acknowledgments

This work is supported by the National Natural Science Foundation of China (No. 51978588). Thanks to Guyuan Chentong Technology Development Co., Ltd., China for providing site support for the experiment.

Author contributions

Rui SU and Qian SU designed the research. Rui SU and Yue LV processed the corresponding data. Rui SU wrote the first draft of the manuscript. Yanfei PEI and Rui SU helped to organize the manuscript. Rui SU and Qian SU revised and edited the final version.

Conflict of interest

Rui SU, Yue LV, Qian SU, and Yanfei PEI declare that they have no conflict of interest.

References

Al-Naghi AAA, Rahman MK, Al-Amoudi OSB, et al., 2020. Thermal performance evaluation of walls with AAC blocks, insulating plaster, and reflective coating. *Journal of Energy Engineering*, 146(2):04019040. https://doi.org/10.1061/(ASCE)EY.1943-7897.0000636

AQSIQ (General Administration of Quality Supervision, Inspection and Quarantine of the People's Republic of China), 2006. Paints and Varnishes—Pull-off Test for Adhesion, GB/T 5210–2006. National Standards of the People's Republic of China (in Chinese).

ASTM (American Society for Testing and Materials), 2012. Standard Specification for Friction Tape, ASTM D4514–12. ASTM, USA.

Chen XH, Zhu Y, Cai DG, et al., 2020. Investigation on interface damage between cement concrete base plate and asphalt concrete waterproofing layer under temperature load in ballastless track. *Applied Sciences*, 10(8):2654. https://doi.org/10.3390/app10082654

Chen YJ, Hu K, Cao SH, 2019. Thermal performance of novel multilayer cool coatings for asphalt pavements. *Materials*, 12(12):1903. https://doi.org/10.3390/ma12121903

Ferrari C, Muscio A, Siligardi C, et al., 2015. Design of a cool color glaze for solar reflective tile application. *Ceramics International*, 41(9):11106-11116. https://doi.org/10.1016/j.ceramint.2015.05.058

Fu QH, Chen XH, Cai DG, et al., 2020. Mechanical characteristics and failure mode of asphalt concrete for ballastless track substructure based on in situ tests. *Applied Sciences*, 10(10):3547. https://doi.org/10.3390/app10103547

Guo W, Qiao X, Huang Y, et al., 2012. Study on energy saving effect of heat-reflective insulation coating on envelopes in the hot summer and cold winter zone. *Energy and Buildings*, 50:196-203. https://doi.org/10.1016/j.enbuild.2012.03.035

Jelle BP, Kalnæs SE, Gao T, 2015. Low-emissivity materials for building applications: a state-of-the-art review and future research perspectives. *Energy and Buildings*, 96:329-356. https://doi.org/10.1016/j.enbuild.2015.03.024

Jiang HL, Zhang JW, Zhou F, et al., 2020. Optimization of PCM coating and its influence on the temperature field of CRTSII ballastless track slab. *Construction and Building Materials*, 236:117498. https://doi.org/10.1016/j.conbuildmat.2019.117498

Jiang L, Wang LC, Wang SY, 2019. A novel solar reflective coating with functional gradient multilayer structure for cooling asphalt pavements. *Construction and Building Materials*, 210:13-21.

https://doi.org/10.1016/j.conbuildmat.2019.03.180

Levinson R, Akbari H, Reilly JC, 2007. Cooler tile-roofed buildings with near-infrared-reflective non-white coatings. *Building and Environment*, 42(7):2591-2605. https://doi.org/10.1016/j.buildenv.2006.06.005

Li Y, Chen JJ, Shi XF, et al., 2021. Thermal performance of the solar reflective fluorocarbon coating and its effects on the mechanical behavior of the ballastless track. *Construction and Building Materials*, 291:123260. https://doi.org/10.1016/j.conbuildmat.2021.123260

Liu P, Zheng ZH, Yu ZW, 2020. Cooperative work of longitudinal slab ballast-less track prestressed concrete simply supported box girder under concrete creep and a temperature gradient. *Structures*, 27:559-569. https://doi.org/10.1016/j.istruc.2020.06.006

Malz S, Krenkel W, Steffens O, 2020. Infrared reflective wall paint in buildings: energy saving potentials and thermal comfort. *Energy and Buildings*, 224:110212. https://doi.org/10.1016/j.enbuild.2020.110212

Park B, Krarti M, 2016. Energy performance analysis of variable reflectivity envelope systems for commercial buildings. *Energy and Buildings*, 124:88-98. https://doi.org/10.1016/j.enbuild.2016.04.070

Saber HH, 2021. Experimental characterization of reflective coating material for cool roofs in hot, humid and dusty climate. *Energy and Buildings*, 242:110993. https://doi.org/10.1016/j.enbuild.2021.110993

SAMR (State Administration for Market Regulation of the People's Republic of China), 2021. General Methods for Preparation of Coating Films, GB/T 1727–2021. National Standards of the People's Republic of China (in Chinese).

Su R, Lv Y, Su Q, et al., 2023. Development of composite-phase change microcapsule coating and numerical investigation on its effect in ballastless track slabs. *Construction and Building Materials*, 375:130974. https://doi.org/10.1016/j.conbuildmat.2023.130974

Thejus PK, Krishnapriya KV, Nishanth KG, 2021. NIR reflective, anticorrosive magenta pigment for energy saving sustainable building coatings. *Solar Energy*, 222:103-114. https://doi.org/10.1016/j.solener.2021.05.017

Yu ZW, Xie Y, Tian XQ, 2019. Research on mechanical performance of CRTS III plate-type ballastless track structure under temperature load based on probability statistics. *Advances in Civil Engineering*, 2019:2975274. https://doi.org/10.1155/2019/2975274

Zeng ZP, Huang ZB, Yin HT, et al., 2018. Influence of track line environment on the temperature field of a double-block ballastless track slab. *Advances in Mechanical Engineering*, 10(12):2975274. https://doi.org/10.1177/1687814018812325

Zhang JW, Jiang HL, Ding F, et al., 2020. Effects of metal-ceramic anticorrosion coating on the performance of ballastless tracks at high temperature. *Archives of Civil and Mechanical Engineering*, 20(4):120. https://doi.org/10.1007/s43452-020-00123-0

Zheng ML, Han LL, Wang F, et al., 2015. Comparison and analysis on heat reflective coating for asphalt pavement based on cooling effect and anti-skid performance. *Construction and Building Materials*, 93:1197-1205. https://doi.org/10.1016/j.conbuildmat.2015.04.043